Fiber-amplifier-enhanced photoacoustic spectroscopy with near-infrared tunable diode lasers

Michael E. Webber, Michael Pushkarsky, and C. Kumar N. Patel

A new approach to wavelength-modulation photoacoustic spectroscopy is reported, which incorporates diode lasers in the near infrared and optical fiber amplifiers to enhance sensitivity. We demonstrate the technique with ammonia detection, yielding a sensitivity limit less than 6 parts in 10^9, by interrogating a transition near 1532 nm with 500 mW of output power from the fiber amplifier, an optical pathlength of 18.4 cm, and an integration time constant of 10 s. This sensitivity is 15 times better than in prior published results for detecting ammonia with near-infrared diode lasers. The normalized minimum detectable fractional optical density, $\alpha_{min}l$, is 1.8×10^{-8}; the minimum detectable absorption coefficient, α_{min}, is 9.5×10^{-10} cm^{-1}; and the minimum detectable absorption coefficient normalized by power and bandwidth is 1.5×10^{-9} W cm$^{-1}/\sqrt{\text{Hz}}$. These measurements represent what we believe to be the first use of fiber amplifiers to enhance photoacoustic spectroscopy, and this technique is applicable to all other species that fall within the gain curves of optical fiber amplifiers.

OCIS codes: 300.6430, 300.6260, 300.6390, 280.3420, 120.6200, 060.2320.

1. Introduction

Significant demand exists for gas-sensing techniques that are fast, sensitive, selective, and compact, and laser-based approaches are attractive because they offer the promise of meeting these criteria. For these systems, diode lasers are popular as sources because they have the beneficial features of narrow linewidth, continuous tunability, compact size, cost effectiveness, room-temperature operation, and compatibility with optical fibers, which enables convenient alignment and multiplexing. However, the most popular telecom lasers that have these features operate at near-infrared wavelengths (generally 1.5–1.65 μm) and therefore overlap with the spectra of vibrational overtones, which are in general 10–200 times weaker than the spectra resulting from fundamental vibrations. To compensate for these small absorption cross sections (line strengths are typically 1×10^{-24} to 1×10^{-25} cm^{-1}/(molecule × cm^{-2}) for most species, though some species have line strengths as high as 1×10^{-21}), many researchers have turned to more-sensitive techniques that work well in the near infrared including (1) cavity ring-down spectroscopy and its variants such as integrated cavity output spectroscopy, which achieve excellent sensitivity through the creation of very long path lengths (kilometers and longer) in a compact volume,[1] (2) autobalancing techniques, which use sophisticated circuitry to reject common-mode electrical and laser-source noises,[2] and (3) frequency-modulation spectroscopy.[3]

Photoacoustic spectroscopy, which is also known to be sensitive for detecting fractional absorbance, has many other attractive features, including compact cell size, ruggedness, simple optical alignment, and inexpensive hearing-aid microphones as transducers. However, the spectroscopic sensitivity of this technique is power dependent, and thus it has been mostly deployed with CO and CO_2 lasers. Despite the many attributes afforded by diode lasers, their low powers (typically less than 25 mW) have prevented their widespread use for photoacoustic spectrometers, and in fact, the authors are aware of less than a dozen published articles to date on this topic, starting with the first introduction by Feher *et al.* in 1994.[4–10] This study presents what to our knowledge is the first implementation of photoacoustic spectroscopy with commercial telecom diode lasers that overcomes the problems of lower power by use of an optical fiber amplifier. Thus the detection benefits of photoacoustic spectroscopy are combined with the performance benefits of diode laser sources to achieve a system that is far more sensitive than prior dem-

The authors are with Pranalytica Inc., 1101 Colorado Avenue, Santa Monica, California 90401. M. E. Webber's e-mail address is webber@pranalytica.com.

Received 21 May 2002; revised manuscript received 22 July 2002.

0003-6935/03/122119-08$15.00/0

onstrated results with near-infrared diode lasers. The new technique is demonstrated with measurements of ammonia, which is a widely used molecule for industrial purposes, a common environmental pollutant, and a biomarker for kidney and liver dysfunction[11] and thus is a valuable target species to monitor. However, the advantages of this technique are applicable to any species with spectral bands that overlap with the wavelengths at which fiber amplifiers operate.

2. Photoacoustic Spectroscopy

Photoacoustic spectroscopy is an attractive gas-sensing technique because of its relative simplicity, ruggedness, and overall sensitivity. As such, many publications are available that describe its principles and various implementations in great detail.[12–15] In brief, photoacoustic spectroscopy is an absorption-based technique that requires modulating the laser output (either in wavelength or amplitude) and then using a microphone to monitor the acoustic waves that occur after the laser radiation is absorbed and converted to local heating by means of collisions and deexcitation in the photoacoustic cell. The magnitude of the measured photoacoustic signal is given by

$$S = S_m PC\alpha\,, \tag{1}$$

where C is a cell-specific constant, in units of pascal centimeters per watt; P is the power of the incident laser radiation, in units of watts; α is the absorption coefficient of the transition that is being interrogated, in inverse centimeters; and S_m is the sensitivity of the microphone, in units of volts per pascal.[16]

The cell-specific constant, C, is a function of cell geometry, measurement cell conditions (pressure and temperature), and the modulation frequency. If the modulation frequency coincides with the resonant frequency of a given mode for an acoustic resonator, stronger photoacoustic signals are achieved as a result of resonant buildup of the sound in the cavity. For this case the cell parameter C is given by

$$C = \frac{(\gamma - 1)LQ}{f_0 V}, \tag{2}$$

where L is the cell length, γ is the ratio of specific heats, V is cell volume, f_0 is the resonant frequency, and Q is a quality factor.[17] The quality factor is defined as the resonant frequency, f_0, normalized by the half-width of the resonance profile, Δf:

$$Q = \frac{f_0}{\Delta f}. \tag{3}$$

The half-width refers to the width of the resonance profile at half the intensity and is measured between the points where the amplitude of the resonance profile is at $1/\sqrt{2}$ the peak value.[14] Q is typically between 10 and 50 for small-diameter longitudinal resonators but can be as high as 1000 for spherical cavities.[18]

Although photoacoustic spectroscopy is often presented as a "zero-baseline" strategy (since to first order, no signal is generated if the target molecules are not present), for implementations that use amplitude modulation of the laser, background "noise" that is coherent with the signal often emerges because of window absorption. Although many sophisticated acoustic cells have been developed to suppress the effects of window noise,[19] its presence typically remains for amplitude-modulated photoacoustic systems, and indeed, is often the limiting factor for detectivity. Moreover, broadband absorption from gas constituents other than the target species may also contribute to the background and impede sensitivity.

Perhaps the most robust technique for eliminating the background signal from broadband absorbers is wavelength-modulation spectroscopy (WMS). When the wavelength of the laser is modulated at a frequency f about the center of the absorption transition, the acoustic signal from wavelength-independent sources such as window absorption and other broadband absorbers (for example, continuum spectra and the wings from interfering species) show up as an offset and thus are eliminated when we evaluate the derivatives of the signal by means of $2f$ demodulation.[4] The laser frequency for WMS is described by

$$\omega_i(t) = \omega_c + a\,\cos(ft)\,, \tag{4}$$

where $\omega_i(t)$ is the instantaneous frequency of the laser, ω_c is the laser's mean frequency, a is the modulation depth, and f is the sinusoidal modulation frequency. For an absorption transition s at half-width at half-maximum denoted as $\Delta\omega$, the wavelength-modulation index m, which is a dimensionless parameter used to describe WMS systems, is defined as [20]

$$m = a/\Delta\omega\,. \tag{5}$$

3. Fiber Amplifiers

Optical fiber amplifiers are the outgrowth of research by the telecommunications industry to transport optical signals over long distances. The basic operating principle is that short lengths of optical fiber, when doped with a small amount of an appropriate rare-earth ion and then pumped with a high-power semiconductor diode, can be used to achieve amplification factors up to 3 orders of magnitude for input signals that occur within the gain band of the dopant.[21]

Although fiber amplifiers can theoretically work at a wide range of wavelengths from 651 nm to longer than 2 μm, depending on the choice of dopant,[21] the most common operating ranges for commercial technology cover the S, C, and L bands in the near infrared. These bands are available by use of fiber amplifiers doped with thulium, ytterbium, erbium, or some combination and have output powers up to 2 W. Table 1 shows the wavelengths for these bands, commercially available output powers, and some species that have spectra within those ranges. Because the telecommunications industry is actively extending

Table 1. Telecommunications Bands, Output Powers, and Species Whose Spectra Overlap with the Wavelength Ranges of the Optical Fiber Amplifier

Band	Wavelength (nm)	Species	Power
S (Short)	1450–1500	H_2O, NH_3	30 mW
C (Conventional)	1520–1570	NH_3, CO, CO_2, HCN, C_2H_2	2 W
L (Long)	1565–1610	CO, CO_2	1 W

the range of wavelengths that it uses, it is reasonable to expect that the coverage by fiber amplifiers will extend to longer wavelengths, thereby offering the opportunity to enhance detection of the first overtone of the C-H stretch for hydrocarbon monitoring. Fiber amplifiers have been used before for spectroscopy, most commonly as a way to improve efficiencies of difference frequency generation to yield milliwatt-level mid-infrared radiation with a Gaussian-beam profile.[22,23] The research in this paper represents the first application of fiber amplifiers to enhance photoacoustic signals for systems operating in the near infrared.

4. Sensor Design

The sensor's schematic is shown in Fig. 1. The tunable diode laser (TDL) operates near 1532 nm with more than 30 dB optical isolation and greater than 20 mW of output power to ensure that the erbium-doped fiber amplifier (EDFA) is fully saturated. Operating in the EDFA's saturation regime prevents unwanted amplification of backreflected radiation, which might damage the laser, and also makes the output power relatively constant, despite small changes to the input power from the seed laser. The ammonia transition near 1532 nm was selected because of its isolation from H_2O and CO_2 interferences (see Fig. 2), line strength, and overlap with the operational range of a *C*-band fiber amplifier.[24,25]

The diode laser is operated in wavelength-modulation mode, whereby it is scanned with a combined sawtooth and sinusoidal waveform. The sawtooth induces the laser to scan slowly (1–10 MHz) in wavelength across the feature of interest, and the sinusoidal waveform dithers the laser's wavelength at half the resonant frequency of the optoacoustic cell's first longitudinal mode (~900 Hz). Although operating the laser this way yields an undesired ramp of the laser's output power from one end of the scan to the other, the fiber amplifier's saturated output removes the effects of these minor input amplitude changes and thus provides nearly constant output power.

The output of the commercially available EDFA, which has up to 500 mW of power with the same linewidth and wavelength as the seed laser, is collimated into free space (N.A. = 0.15; focal length, f_L = 11 mm; beam diameter (BD), <3 mm; angled-physical contact fiber connector) and aligned through the optoacoustic cell with a double-pass configuration to yield a total path length of 18.4 mm. The EDFA unit also has a built-in uncalibrated photodiode for monitoring the relative output power, which is used for normalizing the optoacoustic signal to account for any power changes. The signals from the 5-kHz bandwidth microphones are conditioned and demodulated at twice the modulation frequency by use of a lock-in amplifier (1–10-s time constant) to yield a dc value proportional to the second derivative of the absorption lineshape (see Fig. 3 for sample absorption and 2*f* spectra).

The optoacoustic cell's resonance profile was characterized to determine the frequency of its first longitudinal mode and the value of the cell's quality factor, *Q*, for a range of pressures from 50 to 150 Torr (see Fig. 4). The resonant frequency was twice the modulation frequency at the profile's maximum, and the quality factor was calculated by division of the peak amplitude by the width of the profile where the

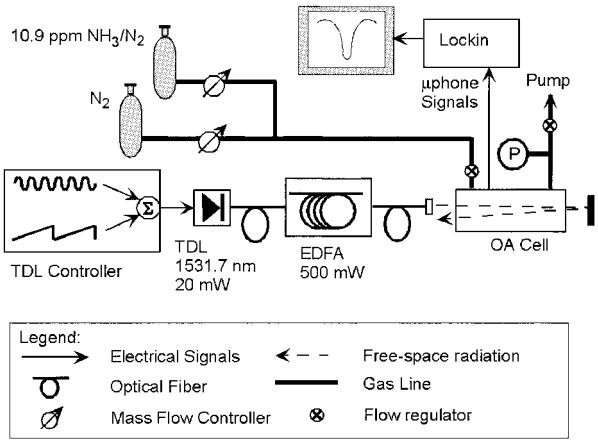

Fig. 1. Experimental schematic for the TDL-OFA photoacoustic sensor. OA, optoacoustic.

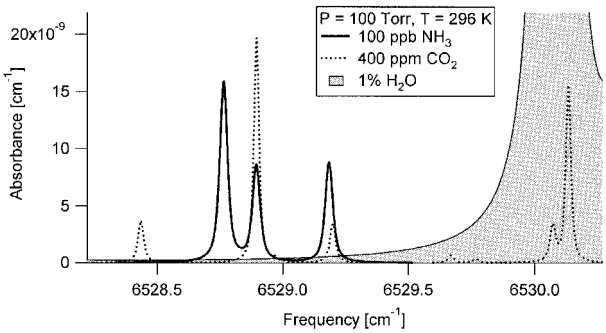

Fig. 2. Ammonia transition at 6528.76 cm^{-1} is isolated from interference from typical background constituents CO_2 and H_2O.[20,21]

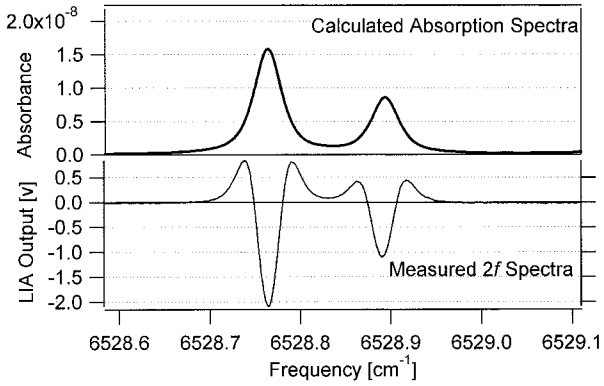

Fig. 3. Calculated absorption spectra based on spectral values from Ref. 20, and measured 2*f* spectra for two ammonia transitions at 6528.76 and 6528.89 cm^{-1}, respectively. LIA, lock-in amplifier.

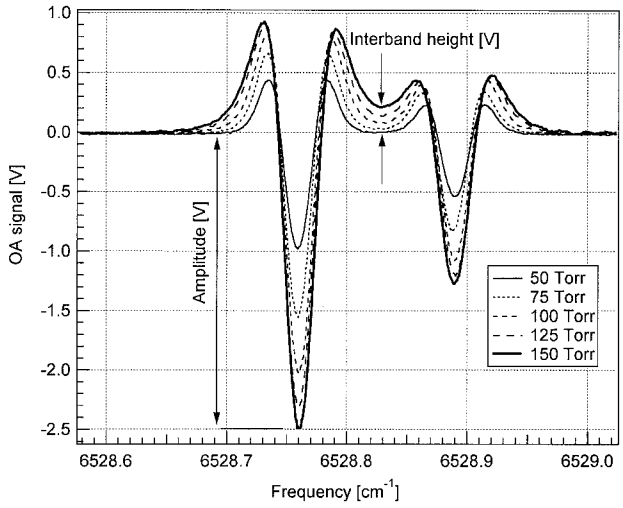

Fig. 5. 2*f* Spectra for different cell pressures from 50 to 150 Torr for 10.9 ppm NH_3 in N_2. The peak amplitude and interband height, which is proportional to the overlap between these neighboring transitions, both increase with pressure.

amplitude had decreased to $1/\sqrt{2}$ of the peak value (the half-intensity value, or 70.7% of the peak). For this optoacoustic cell, the resonant frequency varied from 1770 Hz at 50 Torr up to 1810 Hz at 150 Torr, and Q varied from 32 to 58 over the same range (see the Fig. 4 inset). Clearly, for this cell, higher pressures yield better resonant amplification.

The gas-handling system was composed of a source bottle with a NIST-traceable mixture containing 10.9 parts in 10^6 (ppm) of NH_3 in a balance of N_2, a bottle of N_2 for dilution, and two mass-flow controllers that were used to create mixtures with ammonia concentrations of 100–1000 ppb. Because of ammonia's sticky and corrosive nature, all measurements were made with flowing samples, and appropriate nonadsorptive materials were used wherever possible, including Teflon and quartz. Flow rates between 50 and 100 cm^3/min were used to prevent excessive flow noise resulting from turbulence in the cell.

The signal amplitude and overlap between the neighboring transitions at 6528.76 and 6528.89 cm^{-1} were measured between 50 and 150 Torr to determine the optimum cell pressure for the sensor, with the optimum being the pressure that yields a good compromise between achieving the highest signal but least overlap. The resulting spectra from these tests are plotted in Fig. 5 and clearly illustrate that the peak amplitude increases with pressure. There are two reasons for this trend: (1) as explained above,

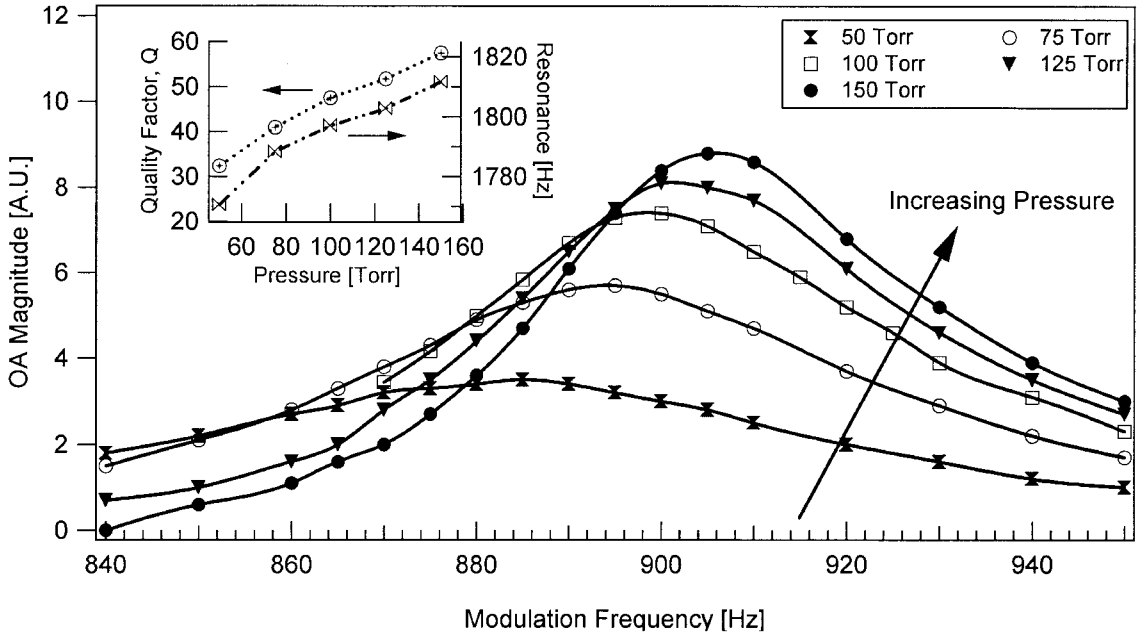

Fig. 4. Resonance profiles of the first longitudinal mode for five different cell pressures at the modulation frequency, which is half the resonance frequency. The inset plots the quality factor, Q, and resonant frequency as a function of pressure. OA, optoacoustic.

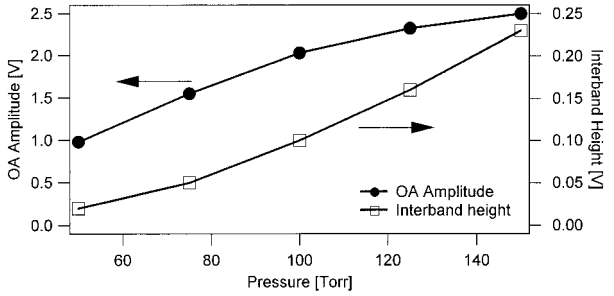

Fig. 6. Signal amplitude and interband height as a function of pressure.

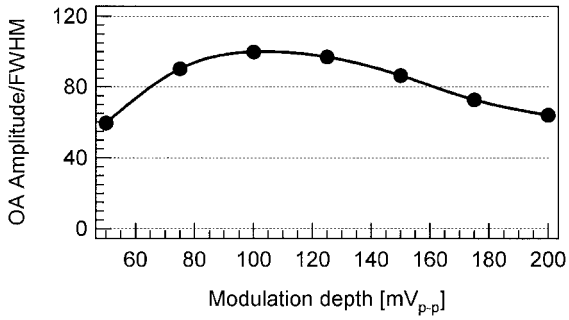

Fig. 8. Ratio of measured peak amplitude and feature width as a function of modulation depth, with a maximum near 100 mV$_{p-p}$.

the amplification factor, Q, increases with pressure, and (2) the peak of the lineshape, which is affected by both Doppler and collisional broadening, increases with the partial pressure of ammonia. Although increasing pressures yield higher signals, the overlap between the neighboring transitions, indicated in Fig. 6 as interband height, also increases, thereby limiting the instrument's interference rejection. For this system, the optimum pressure was determined to be 100 Torr, which is consistent with prior determinations for the best measurement pressure to use when ammonia is monitored with direct absorption to accomplish the same goal of maximizing signal and isolation.[26]

For wavelength-modulation spectroscopy, an important sensor design parameter is the modulation depth for dithering the laser's wavelength. In an analogous fashion to the pressure tests described above, spectra were recorded for different modulation depths, from 50 to 200 mV peak-to-peak (mV$_{p-p}$), to determine the optimum condition that yields the best balance between signal magnitude and highest resolution (the current controller transfer function is 20 mA/V). The spectra from these measurements are shown in Fig. 7 for 10.9 ppm NH_3 at a cell pressure of 100 Torr, with the modulation depth increasing in 25-mV$_{p-p}$ increments for successive measurements. As can be seen from this plot, the peak signal magnitude mostly increases with modulation, whereas the widths and overlap of the transitions also increases. Figure 8 shows the ratio of signal amplitude and linewidth for varying modulation depths, which reveals that a modulation of 100 mV$_{p-p}$ (2 mA) yields the highest ratio, and thus was determined to be the best condition to use with this sensor. For this particular laser, 2 mA corresponds to a peak-to-peak modulation depth of $2a = 0.053\ cm^{-1}$. With a Voigt FWHM linewidth evaluated to be $0.036\ cm^{-1}$ for this transition at room temperature and 100 Torr, the modulation index is then 1.47. This index is lower than a typical value of 2.2–2.4 that is used to maximize signal[20] but is very similar to a prior published value of 1.46 used to maximize both signal and isolation for measurements of CO.[27]

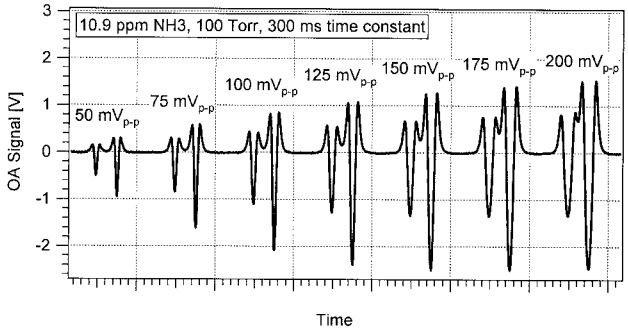

Fig. 7. Successive scans of the two ammonia transitions near 1531.7 nm with modulation depths varying in 25-mV$_{p-p}$ increments.

5. Results and Discussion

The sensor was operated according to the optimum design conditions that were determined beforehand and explained above, namely, at a pressure of 100 Torr, with a modulation depth of 2 mA, and at a modulation frequency equal to half the resonant frequency of the cell, which was roughly 1800 Hz. The sensor was used to measure the ammonia mixture after dilution with N_2 by a factor of 100, to yield a flow with an ammonia concentration of roughly 110 ppb. The measured spectra for this condition are shown in Fig. 9 and have signal-to-noise ratio equal to slightly more than 19. The noise is estimated to be the standard deviation of the optoacoustic signal at an off-resonant wavelength, as shown in the graph, but because the sensitivity-limiting noise appears oscillatory or nonstochastic in nature, the standard deviation is a less meaningful indicator of noise, and thus it serves only as a useful metric for comparing this study with other prior publications. A stricter test of the minimum detectivity for this study and similar efforts is the replicate precision of successive measurements when the sensor is exposed to the same known gas concentration over a statistically significant period of time. The source of the noise at off-resonance wavelengths is unknown to the authors at this time. Its oscillatory pattern is consistent with interference fringes from optical components in the measurement path or from residual amplitude modulation from within the fiber amplifier, but since the photoacoustic technique monitors acoustic power in-

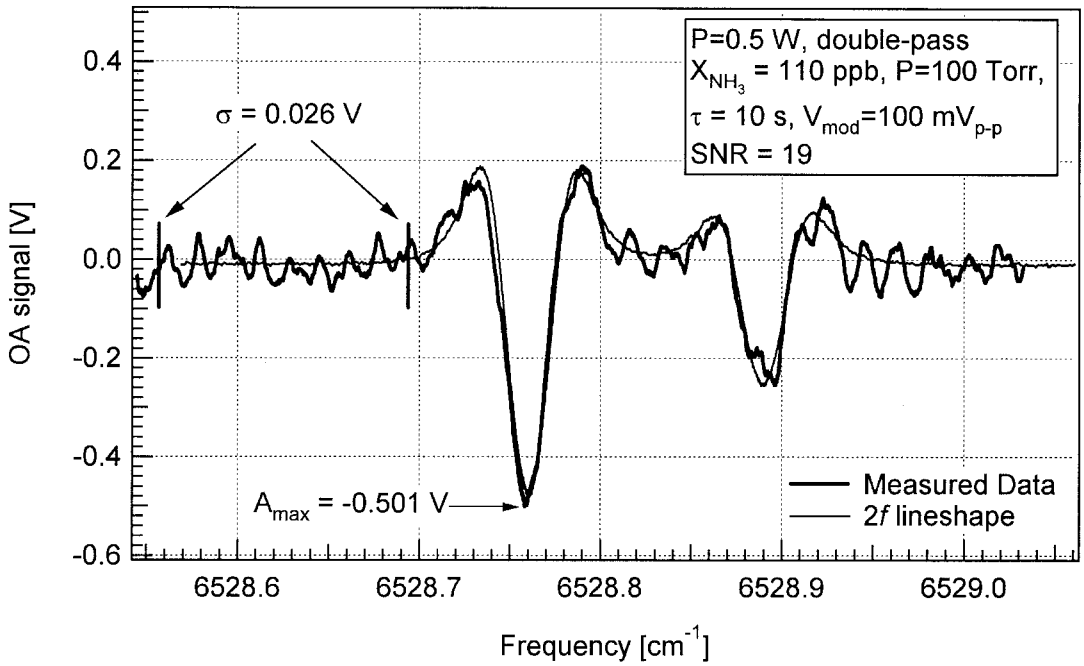

Fig. 9. Measured 2*f* spectra of 110 ppb flowing NH_3 in N_2, at optimum conditions, with SNR = 19.

stead of laser power, it is insensitive to optical fringes, and thus the authors suspect that the noise is electrical in nature.

This signal-to-noise ratio indicates that the 1σ noise-limited detection limit for this sensor is better than 6 ppb of ammonia, which is superior to the detection limit that has been achieved with any other published near-infrared diode laser system, to the best of the authors' knowledge. This sensitivity was achieved with 500 mW of power, a pathlength of 18.4 cm, and a lock-in time constant of 10 s. Thus the normalized minimum detectable fractional optical density, $\alpha_{min}l$, is calculated to be 1.8×10^{-8}; the minimum detectable absorption coefficient, α_{min}, is 9.5×10^{-10} cm^{-1}; and the minimum detectable absorption coefficient normalized by power and bandwidth is 1.5×10^{-9} W $cm^{-1}/\sqrt{Hz}$. Assuming that the noise is nonoptical in nature, the sensitivity of this system can readily be enhanced by use of a 1-W fiber amplifier and a multipass system to achieve sub-ppb detection limits, and this research is already in progress. For comparison, Schmohl *et al.*[28] used diode-laser-based photoacoustic spectroscopy to measure the same ammonia transition and achieved a minimum detectable absorption of 3.4×10^{-8} cm^{-1}. As delineated in Table 3, our minimum detection limit is at least 15 times better than the results obtained with other diode laser techniques to interrogate the same transitions at 1531 nm.

Table 2. Results for This Sensor Compared with Recent Publications on Ammonia Detection That Used the Same Transitions near 1531 nm as Were Used for This Study

Technique	Minimum Detectivity (ppb)	Year	Reference
Photoacoustic and WMS	6	2002	This study
Photoacoustic	200	2002	28
Cavity-enhanced absorption spectroscopy	100	2000	29
Direct absorption with multipass cell	280	2001	30
Direct absorption with multipass cell	700	2001	31

Table 3. Detection Limits for This Sensor When Applied to Detecting Other Species, the Detection Wavelength, and the Transition Line Strength

Species	Inferred Detection Limit	λ (nm)	Line Strength (cm^{-2} atm^{-1})
NH_3	6 ppb	1531.68 (Ref. 24)	0.0624 (Ref. 24)
C_2H_2	2.6 ppb	1531.588 (Ref. 32)	0.143 (Ref. 32)
HCN	3.4 ppb	1539.698 (Ref. 33)	0.112 (Ref. 33)
CO_2	51 ppm	1598.806 (Ref. 25)	7.29e-6 (Ref. 25)
CO	650 ppb	1568.036 (Ref. 25)	5.72e-4 (Ref. 25)

Although the design techniques described above were demonstrated with ammonia detection, in principle they are applicable to any species whose spectra overlap with the wavelengths of fiber amplifiers. Other species are listed in Table 2, along with the line strength, wavelength, and inferred detection limit when measured with this sensor. For some species, such as acetylene and hydrogen cyanide, the maximum line strengths within the range of the fiber amplifiers are approximately 40 and 80 times weaker, respectively, than those at the fundamental near 3.0 μm. But since the output powers available with EDFAs are hundreds of times higher than what is currently available with mid-infrared sources, it can be advantageous to perform photoacoustic measurements in the near infrared despite the weaker transitions. For example, using 500 mW at 1540 nm to measure HCN would yield sensitivity more than 6 times better than using 1 mW at 3 μm.

6. Conclusions

A gas sensor was developed by use of diode lasers, fiber amplifiers, wavelength modulation, and resonant photoacoustic spectroscopy to yield a detection limit for ammonia of less than 6 ppb. This technique represents what we believe to be the first use of fiber amplifiers to enhance photoacoustic detection in the near infrared, and yielded detection limits for ammonia that are more than 15 times better than in other prior published studies using near-infrared diode lasers. Although this system was demonstrated for ammonia, it is applicable to any other species with spectra within the range of the fiber amplifiers.

References

1. J. B. Paul, L. Lapson, and J. G. Anderson, "Ultrasensitive absorption spectroscopy with a high-finesse optical cavity and off-axis alignment," Appl. Opt. **40,** 4901–4910 (2001).
2. P. C. D. Hobbs, "Ultrasensitive laser measurements without tears," Appl. Opt. **36,** 903–920 (1997).
3. J. A. Silver, "Frequency modulation spectroscopy for trace species detection: theory and comparison among experimental methods," Appl. Opt. **31,** 707–717 (1992).
4. M. Feher, J. Jian, J. P. Maier, and A. Miklos, "Optoacoustic trace-gas monitoring with near-infrared diode lasers," Appl. Opt. **33,** 1655–1658 (1994).
5. A. Miklos and M. Feher, "Optoacoustic detection with near-infrared diode lasers: trace gases and short-lived molecules," Infrared Phys. Technol. **37,** 21–27 (1996).
6. S. Schafer, M. Mashni, J. Sneider, A. Miklos, P. Hess, H. Pitz, K.-U. Pleban, and V. Ebert, "Sensitive detection of methane with a 1.65 μm diode laser by photoacoustic and absorption spectroscopy," Appl. Phys. B **66,** 511–516 (1998).
7. Z. Bozoki, J. Sneider, Z. Gingl, A. Mohacsi, M. Szakll, Z. Bor, and G. Szabo, "A high-sensitivity, near-infrared tunable-diode-laser-based photoacoustic water-vapour-detection system for automated operation," Meas. Sci. Technol. **10,** 999–1003 (1999).
8. B. A. Paldus, T. G. Spence, R. N. Zare, J. Oomens, F. J. M. Harren, D. H. Parker, C. Gmachl, F. Cappasso, D. L. Sivco, J. N. Gaillargeon, A. L. Hutchinson, and A. Y. Cho, "Photoacoustic spectroscopy using quantum-cascade lasers," Opt. Lett. **24,** 178–180 (1999).
9. A. Boschetti, D. Bassi, E. Iacob, S. Iannotta, L. Ricci, and M. Scotoni, "Resonant photoacoustic simultaneous detection of methane and ethylene by means of a 1.63-μm diode laser," Appl. Phys. B **74,** 273–278 (2002).
10. D. Hofstetter, M. Beck, J. Faist, M. Nagele, and M. W. Sigrist, "Photoacoustic spectroscopy with quantum cascade distributed-feedback lasers," Opt. Lett. **26,** 887–889 (2001).
11. L. R. Narasimhan, W. Goodman, and C. K. N. Patel, "Correlation of breath ammonia with blood urea nitrogen and creatinine during hemodialysis," Proc. Natl. Acad. Sci. **98,** 4617–4621 (2001).
12. P. Hess, ed., *Topics in Current Physics: Photoacoustic, Photothermal and Photochemical Processes in Gases* (Springer-Verlag, Berlin, 1989).
13. P. Repond and M. W. Sigrist, "Photoacoustic spectroscopy on trace gases with continuously tunable CO_2 laser," Appl. Opt. **35,** 4065–4085 (1996).
14. A. Miklos and P. Hess, "Application of acoustic resonators in photoacoustic trace gas analysis and metrology," Rev. Sci. Instrum. **72,** 1937–1955 (2001).
15. S. Schafer, A. Miklos, and P. Hess, "Quantitative signal analysis in pulsed resonant photoacoustics," Appl. Opt. **36,** 3202–3211 (1997).
16. W. Demtroder, *Laser Spectroscopy: Basic Concepts and Instrumentation*, 2nd ed. (Springer-Verlag, Berlin, 1996).
17. A. Rosencwaig, *Photoacoustics and Photoacoustic Spectroscopy* (Wiley, New York, 1980).
18. J. Henningsen and N. Melander, "Sensitive measurement of adsorption dynamics with nonresonant gas phase photoacoustics," Appl. Opt. **36,** 7037–7045 (1997).
19. F. G. C. Bijnen, J. Reuss, and F. J. M. Harren, "Geometrical optimization of a longitudinal resonant photoacoustic cell for sensitive and fast trace gas detection," Rev. Sci. Instrum. **67,** 2914–2923 (1996).
20. S.-I. Chou, D. S. Baer, R. K. Hanson, W. Z. Collison, and T. Q. Ni, "HBr concentration and temperature measurements in a plasma etch reactor using diode laser absorption spectroscopy," J. Vac. Sci. Technol. A **19,** 477–484 (2001).
21. P. W. France, ed., *Optical Fibre Lasers and Amplifiers* (CRC Press, Boca Raton, Fla., 1991).
22. D. Richter, D. G. Lancaster, and F. K. Tittel, "Development of an automated diode-laser-based multicomponent gas sensor," Appl. Opt. **39,** 4444–4450 (2000).
23. D. Richter, A. Fried, B. P. Wert, J. G. Walega, and F. K. Tittel, "Development of a tunable mid-IR difference-frequency laser source for highly-sensitive airborne trace gas detection," Appl. Phys. B **75,** 281–288 (2002).
24. M. E. Webber, D. S. Baer, and R. K. Hanson, "Ammonia monitoring near 1.5 μm with diode-laser absorption sensors," Appl. Opt. **40,** 2031–2042 (2001).
25. L. S. Rothmann, C. P. Rinsland, A. Goldman, S. T. Massie, D. P. Edwards, J.-Y. Mandin, J. Schroeder, A. McCann, R. R. Gamache, R. B. Wattsin, K. Yoshino, K. V. Chance, K. W. Juck, L. R. Brown, V. Nemtchechin, and P. Varanasi, "The HITRAN molecular spectroscopic database and HAWKS (HITRAN atmospheric workstation): 1996 edition," J. Quant. Spectrosc. Radiat. Transfer **60,** 710 (1998).
26. M. E. Webber, R. Claps, F. V. Englich, F. K. Tittel, J. B. Jeffries, and R. K. Hanson, "Measurements of NH_3 and CO_2 with distributed-feedback diode lasers near 2.0 μm in bioreactor vent gases," Appl. Opt. **40,** 4395–4403 (2001).
27. J. Wang, M. Maiorov, D. S. Baer, D. Z. Barbuzov, J. C. Connolly, and R. K. Hanson, "*In-situ* combustion measurements of CO with diode-laser absorption near 2.3 μm," Appl. Opt. **39,** 5579–5589 (2000).
28. A. Schmohl, A. Miklos, and P. Hess, "Detection of ammonia by photoacoustic spectroscopy with semiconductor lasers," Appl. Opt. **41,** 1815–1823 (2002).

29. R. Peeters, G. Berden, A. Apituley, and G. Meijer, "Open-path trace gas detection of ammonia based on cavity-enhanced absorption spectroscopy," Appl. Phys. B **71,** 231–236 (2000).
30. D. P. Leleux, R. Claps, W. Chen, F. K. Tittel, and T. L. Harman, "Applications of Kalman filtering to real-time trace gas concentration measurements," Appl. Phys. B **74,** 85–93 (2002).
31. R. Claps, F. V. Englich, D. P. Leleux, D. Richter, F. K. Tittel, and R. F. Curl, "Ammonia detection by use of near-infrared diode-laser-based overtone spectroscopy," Appl. Opt. **40,** 4387–4394 (2001).
32. "High resolution wavelength calibration reference for 1510 nm–1540 nm acetylene $^{12}C_2H_2$," National Institute of Standards and Technology, Certificate, Standard Reference Material 2517a, December 11, 2000.
33. N. Jacquinet-Husson, E. Arie, J. Ballard, A. Barbe, G. Bjoraker, B. Bonnet, L. R. Brown, C. Camy-Peyret, J. P. Champion, A. Chedin, A. Chrusin, C. Clerbaux, G. Duxbury, J.-M. Flaud, N. Fourrie, A. Fayt, G. Graner, R. Gamache, A. Goldman, V. Golovko, G. Guelachvili, J.-M. Hartmann, J. C. Hilico, J. Hillman, G. Lefevre, E. Lellouch, S. N. Mikhailenko, O. V. Naumenko, V. Nemtchinov, D. Newnham, A. Nikitin, J. Orphal, A. Perrin, D. C. Reuter, C. P. Rinsland, L. Rosenmann, L. S. Rothman, N. A. Scott, J. Selby, L. N. Sinitsa, J. M. Sirota, A. M. Smith, K. M. Smith, V. G. Tyuterev, R. H. Tipping, S. Urban, P. Varanasi, and M. Weber, "The 1997 spectroscopic GEISA databank," J. Quant. Spectrosc. Radiat. Transfer **62,** 205–254 (1999).